

# Physically Interpretable World Models via Weakly Supervised Representation Learning

Zhenjiang Mao  
University of Florida  
Gainesville, USA

Mrinall Eashaan Umasudhan  
University of Florida  
Gainesville, USA

Ivan Ruchkin  
University of Florida  
Gainesville, USA

## Abstract

Learning predictive models from high-dimensional sensory observations is fundamental for cyber-physical systems, yet the latent representations learned by standard world models lack physical interpretability. This limits their reliability, generalizability, and applicability to safety-critical tasks. We introduce Physically Interpretable World Models (PIWM), a framework that aligns latent representations with real-world physical quantities and constrains their evolution through partially known physical dynamics. Physical interpretability in PIWM is defined by two complementary properties: (i) the learned latent state corresponds to meaningful physical variables, and (ii) its temporal evolution follows physically consistent dynamics. To achieve this without requiring ground-truth physical annotations, PIWM employs weak distribution-based supervision that captures state uncertainty naturally arising from real-world sensing pipelines. The architecture integrates a VQ-based visual encoder, a transformer-based physical encoder, and a learnable dynamics model grounded in known physical equations. Across three case studies (Cart Pole, Lunar Lander, and Donkey Car), PIWM achieves accurate long-horizon prediction, recovers true system parameters, and significantly improves physical grounding over purely data-driven models. These results demonstrate the feasibility and advantages of learning physically interpretable world models directly from images under weak supervision.

## CCS Concepts

• **Computing methodologies** → **Learning latent representations**; • **Computer systems organization** → **Embedded and cyber-physical systems**.

## Keywords

Interpretable Representation Learning, Trajectory Prediction, World Models, Physics-Informed Machine Learning, Autonomous Systems

## ACM Reference Format:

Zhenjiang Mao, Mrinall Eashaan Umasudhan, and Ivan Ruchkin. 2025. Physically Interpretable World Models via Weakly Supervised Representation Learning. In *Proceedings of (Arxiv)*. ACM, New York, NY, USA, 14 pages. <https://doi.org/10.1145/nnnnnnn.nnnnnnn>

Permission to make digital or hard copies of all or part of this work for personal or classroom use is granted without fee provided that copies are not made or distributed for profit or commercial advantage and that copies bear this notice and the full citation on the first page. Copyrights for components of this work owned by others than the author(s) must be honored. Abstracting with credit is permitted. To copy otherwise, or republish, to post on servers or to redistribute to lists, requires prior specific permission and/or a fee. Request permissions from [permissions@acm.org](mailto:permissions@acm.org).

Arxiv, 2025

© 2025 Copyright held by the owner/author(s). Publication rights licensed to ACM. <https://doi.org/10.1145/nnnnnnn.nnnnnnn>

## 1 Introduction

Accurate and robust trajectory prediction from high-dimensional sensor data, such as camera images, is a fundamental challenge for the safe operation of cyber-physical systems (CPS). A dominant paradigm for this task is to learn compact latent representations of the environment and evolve them over time. This idea underlies modern *world models* [15], which typically combine deep visual encoders with predictive temporal models such as RNNs or transformers [17, 39, 49]. While these models achieve strong long-horizon prediction performance, their latent representations usually function as a “black box,” lacking a clear connection to the underlying physical state of the system.

Such a gap limits trustworthiness, controllability, and safety in CPS. In settings like autonomous driving or household robotics, physically meaningful latent states enable causal explanations (e.g., slowing down due to occlusions) and support high-assurance methodologies such as formal verification [18, 25] and run-time shielding [1, 55]. If predicted states can be mapped to interpretable quantities such as position or velocity, a safety monitor can detect unsafe future configurations (e.g., entering an occupied lane) and intervene accordingly. Furthermore, embedding physical structure into the latent space improves generalization by constraining predictions to physically plausible trajectories.

Existing attempts to learn physically interpretable latents from images generally fall into two paradigms, illustrated in Figure 1. *Extrinsic* approaches first learn abstract visual latents and then map them to physical quantities via an additional model. *Intrinsic* approaches instead attempt to encode physical structure directly within the image encoder, enforcing that the latent representation itself corresponds to meaningful physical variables. While effective in controlled settings [29], both paradigms typically *require exact physical labels* during training or rely on object-centric decompositions [41], which are difficult to reliably obtain from real-world CPS.

We aim to overcome this limitation by learning physical representations *without exact physical supervision*. In many CPS, sensors such as GPS and radar naturally produce uncertain estimates in the form of distributions or confidence intervals rather than precise measurements. These distributional signals provide coarse yet informative constraints. For example, approximate position ranges or speed bounds that reflect the true physical state while tolerating noise and ambiguity. We leverage such distribution-based weak supervision to guide the encoding of high-dimensional images toward physically meaningful latent states. Combined with partially known system dynamics (which is also typical for CPS), this enables physically consistent multi-step prediction without requiring access to ground-truth states.

To this end, we propose the *Physically Interpretable World Model (PIWM)*, a framework that learns latent states aligned with real

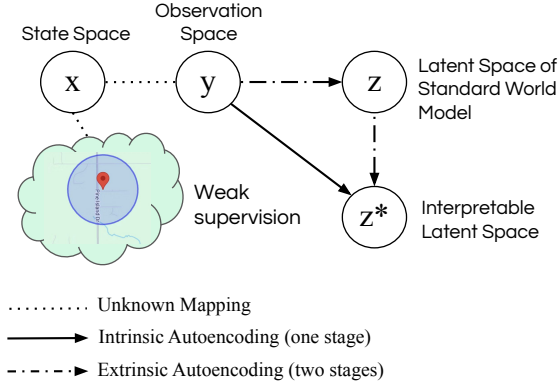


**Figure 1: Conceptual illustration of learning physically meaningful latent spaces from images.** High-dimensional observations  $y$  may be encoded into a standard latent space  $z$  or an interpretable latent space  $z^*$ . Weak supervision vaguely relates observations to the underlying physical state  $x$ . Existing approaches follow two paradigms: *intrinsic* autoencoding (one-stage) and *extrinsic* autoencoding (two-stage).

physical quantities and constrains their temporal evolution using a structured, partially known dynamics model. In this work, *physical interpretability* encompasses two complementary properties: (i) some latent dimensions correspond to meaningful physical variables, and (ii) latent evolution follows physically consistent dynamics. PIWM provides a general architectural template that combines image-based representation learning, physically interpretable latent spaces, and physics-informed dynamics. Rather than prescribing a single architecture, PIWM defines a design space that can be instantiated with intrinsic or extrinsic encoders, and with continuous or discrete latent parameterizations. Within this space, physical interpretability arises from aligning latent variables with weak supervision and constraining their temporal evolution through structured dynamics. Simultaneously, weak distributional supervision enforces alignment between latent states and physical quantities, eliminating reliance on the exact ground truth for training.

We conduct an extensive experimental study to answer a central question: *How can weak supervision and latent quantization make world models physically interpretable?* We systematically examine continuous versus discrete latent spaces as well as intrinsic versus extrinsic designs. Across three case studies – CartPole, Lunar Lander, and the DonkeyCar autonomous racing platform – PIWM achieves superior physical grounding and long-horizon prediction accuracy compared to purely data-driven models and baselines. Notably, extrinsic architectures with quantized latent spaces consistently yield the most physically plausible and robust representations, highlighting the importance of decoupling visual encoding from physical interpretation.

Thus, this paper makes three contributions:

- (1) **A unified definition of physical interpretability.** We formalize physical interpretability for generative world models as two complementary properties: (i) latent representations

correspond to meaningful physical quantities, and (ii) their temporal evolution obeys physically valid dynamics.

- (2) **A novel weakly supervised framework for learning physically grounded latents.** We introduce an architecture and training pipeline that aligns image-based latent states with physical variables using *distribution-based weak supervision* instead of exact physical annotations. It also makes use of additional physical priors in the form of structural dynamics and latent quantization.
- (3) **A systematic empirical study of latent design choices.** Through extensive experiments on CartPole, Lunar Lander, and DonkeyCar, we analyze intrinsic vs. extrinsic architectures and continuous vs. discrete latents. The results reveal that *extrinsic architectures with quantized latents* consistently achieve the most robust and interpretable representations, outperforming data-driven baselines in long-horizon prediction and physical parameter recovery.

The remainder of this paper is organized as follows. Section 2 introduces the necessary background on autonomous systems, world models, and learned representations. Section 3 presents the proposed framework, including the representation learning module, the structured dynamics model, and the unified training procedure. Section 4 reports an extensive empirical study across three case studies, evaluating predictive performance, physical interpretability, and the effects of latent design choices. Section 5 discusses our findings, whereas Section 6 reviews the existing work. Finally, Section 7 concludes the paper.

## 2 Preliminaries

### 2.1 Autonomous system and world models

**DEFINITION 1 (AUTONOMOUS CPS).** An autonomous CPS  $s = (X, I, Y, A, \phi_\theta, g, h)$  models the evolution of an perception-based control system, where the state set  $X$  defines the finite-dimensional space of physical states, the initial set  $I \subset X$  specifies possible starting states, observation set  $Y$  contains all possible observations, and the action set  $A$  contains available control actions. The system dynamics  $\phi_\theta : X \times A \times \Theta \rightarrow X$  governs state transitions under physical parameters  $\theta \in \Theta$ , the observation function  $g : X \rightarrow Y$  maps states to observations, and the fixed controller  $h : Y \rightarrow A$  selects actions based on observations.

We consider an autonomous system with observation-based control, the states of which evolve as  $x_{t+1} = \phi(x_t, a_t, \theta^*)$ , where  $\theta^*$  are the true (unknown) physical parameters. The known controller  $h$  relies on observations  $y$  from sensors (e.g., cameras). Such controllers can be trained by imitation learning [21] or reinforcement learning [23, 33], and we assume that it has been done for our purposes. Given an initial state  $x_0 \in I$ , a *state trajectory* is defined by iteratively applying the dynamics function  $\phi$ , yielding a sequence  $(x_0, x_1, \dots, x_t)$ , where each state is  $x_{t+1} = \phi(x_t, a_t, \theta^*)$  and the action is generated by the controller based on the observation:  $a_t = h(y_t) = h(g(x_t))$ . Correspondingly, an *observation trajectory*  $(y_0, y_1, \dots, y_t)$  is generated by applying the observation function  $g$  to each state:  $y_t = g(x_t)$ .

We consider the setting where the state is not directly observable, and to anticipate hazards and adapt, the system needs to forecast

observations. This is done by combining a world model conditioned on past observations with an observation-based controller  $h$ , essentially forming an efficient online simulator of future observations.

**DEFINITION 2 (WORLD MODEL).** A world model  $\mathcal{W} = (\mathcal{E}, f, \mathcal{D})$  predicts the future evolution of observations in an autonomous CPS  $s$ , where the encoder  $\mathcal{E} : Y \rightarrow Z$  compresses high-dimensional observations into latent representations, the predictor  $f : Z \times A \rightarrow Z$  forecasts future latents conditioned on actions, and the decoder  $\mathcal{D} : Z \rightarrow Y$  reconstructs predicted observations. The actions  $a_t$  are generated by a controller  $h : Y \rightarrow A$  based on the current observation  $y_t$ , and together with the encoded latent  $z_t = \mathcal{E}(y_t)$ , are used to obtain the future latent  $z_{t+1} = f(z_t, a_t)$ . The predicted observation  $\hat{y}_{t+1}$  is then obtained by decoding  $z_{t+1}$  with  $\mathcal{D} : \hat{y}_{t+1} = \mathcal{D}(z_{t+1})$ .

While world models enable diverse tasks (e.g., controller training, monitoring, and planning), they are usually evaluated with *predictive accuracy* – how closely the predicted observations  $\hat{y}_{t+1:t+n}$  match the true observations  $y_{t+1:t+n}$ . The typical metrics include mean squared error (MSE) and structural similarity index (SSIM). Unfortunately, these metrics are inherently limited: similar pixel-wise observations may correspond to very different underlying states. This means that the similarity (low MSE and high SSIM) between  $\hat{y}_{t+1:t+n}$  and  $y_{t+1:t+n}$  does not guarantee similarity between the underlying physical states corresponding to the predicted observations and the true physical ones. Thus, the error in predicted observations is *not physically interpretable*. This severely limits the predictions’ utility for downstream CPS tasks like safety monitoring and planning. Instead, we turn our attention to the latent states.

## 2.2 Interpretable Latent Representations

The autoencoder components  $\mathcal{E}$  and  $\mathcal{D}$  in world models are primarily based on Variational Autoencoders (VAEs), Vector-Quantized Variational Autoencoder (VQ-VAEs), or their variants. VAEs [27] encode high-dimensional inputs  $y$  into continuous latent vectors  $z = \mathcal{E}(y)$ , which are then decoded back into reconstructed inputs  $\hat{y} = \mathcal{D}(z)$ . A standard VAE assumes a simple prior distribution over the latent space, typically an isotropic Gaussian, which facilitates tractable inference but imposes a strong inductive bias. A VQ-VAE [53] discretizes the latent space by mapping a high-dimensional observation  $y_t$  to a continuous latent vector  $z_t = \mathcal{E}(y_t)$ , then quantizing it via a *codebook*  $\{e_k\}_{k=1}^K$  to obtain a discrete latent index  $z_t^* = \arg \min_k \|z_t - e_k\|_2^2$  closest to the continuous latent  $z_t$ . The decoder then reconstructs the observation via  $\hat{y}_t = \mathcal{D}(e_{z_t^*})$ . While discretization introduces structure and regularization, the learned codebook vectors  $e_k$  themselves are typically unstructured and lack interpretation. Therefore, merely discretizing the space is insufficient: an explicit mechanism is needed to align these latent representations with physical semantics.

Our setting assumes that general knowledge about the dynamics function  $\phi$ , namely the structure of its equations. However, the dynamics parameters  $\theta$ , such as the mass or friction coefficient, are unknown, making the system  $s$  only partially specified. In practice, it is often hard to find the true parameters  $\theta^*$  because true physical states  $x$  cannot be measured precisely. However, it is typical to compute a *distribution*  $p(x)$  from high-dimensional observations. For instance, the robot’s pose may be estimated from images as a range/distribution – and serve as a weak supervisory signal.

Thus, to train a world model, we are given a dataset  $\mathcal{S}$  of trajectories, consisting of  $N$  sequences of length  $M$ , where each sequence contains tuples of images, actions, and state distribution labels:

$$\mathcal{S} = \left\{ (y_{1:M}, a_{1:M}, p_{1:M}(x)) \right\}_{1:N} \quad (1)$$

The weak supervision is provided by state distributions  $p_t(x)$ , for which we assume no analytical form is known. Instead, we can only draw a finite set of samples from them. This represents a challenging yet practical scenario, as it is a weaker assumption than knowing the distribution’s type (e.g., Gaussian), its parameters (e.g., mean and variance), or a definitive interval.

Our ultimate task is to learn a representation  $z^*$  that accurately approximates the system’s true, unobserved physical state  $x$  for prediction. We formalize this as two distinct but related problems:

**DEFINITION 3 (INTERPRETABLE REPRESENTATION LEARNING PROBLEM).** Given a dataset  $\mathcal{S}$  and a controller  $h$ , the objective is to learn a state representation  $z^* = \mathcal{E}(y)$  that minimizes the mean squared error to the true physical state  $x$ :

$$\min_{\mathcal{E}} \mathbb{E} [\|x - \mathcal{E}(y)\|_2^2] \quad (2)$$

Next, the prediction problem is to forecast the evolution of these interpretable representations over time:

**DEFINITION 4 (PREDICTION PROBLEM FOR INTERPRETABLE REPRESENTATIONS).** Given a dataset  $\mathcal{S}$ , a dynamics function  $\phi$  with unknown parameters, and a controller  $h$ , the objective is to train a predictor that maps a history of representations to a future representation,  $\hat{z}_{t+H}^* = \mathcal{P}(z_{-m:t}^*)$ , by minimizing the future prediction error:

$$\min_{\mathcal{P}} \mathbb{E} [\|x_{t+H} - \hat{z}_{t+H}^*\|_2^2]. \quad (3)$$

The objectives in Definitions 3 and 4 are formulated with respect to the true physical state  $x$ , which serves as the ultimate ground truth for evaluating physical interpretability. However, since  $x$  is not accessible during training, these objectives cannot be optimized directly. Our proposed method, detailed in Section 3, addresses this challenge by constructing a tractable surrogate objective that leverages the weak supervision by sampling state distributions  $p(x)$ . Throughout this paper, we use calligraphic letters (e.g.,  $\mathcal{E}$ ,  $\mathcal{D}$ ,  $\mathcal{S}$ ) to denote functions and datasets for clarity. During training, we optimize model parameters  $w$  using mini-batch gradient descent with batch size  $B$ , learning rate  $\eta$ , and train for  $n_{\text{epochs}}$  epochs.

*Noise Model.* Since the true physical state  $x$  is not directly observable, the weak supervision available during training consists of samples drawn from an unknown distribution  $p(x)$  obtained from noisy sensor data. We assume only that  $p(x)$  provides a *mean-proximal* estimate of each state dimension. For the  $i$ -th state component, let  $\mathcal{X}_i$  denote the valid range size of that dimension. Then the weak supervision is such that the true value  $x_i$  lies within an interval of relative width  $\delta$  centered at the distributional mean:

$$x_i \in \left[ \mathbb{E}[p(x)] - \frac{1}{2}\delta |\mathcal{X}_i|, \mathbb{E}[p(x)] + \frac{1}{2}\delta |\mathcal{X}_i| \right].$$

Here, hyperparameter  $\delta \in (0, 1)$  quantifies the weakness of the supervision. This interval characterizes the feasible set from which

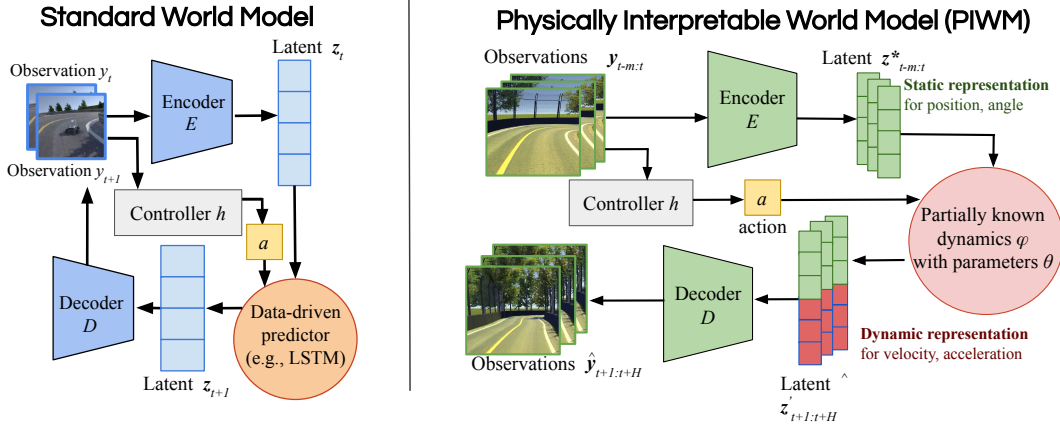


**Figure 2: Overview of world model architectures. (Left) Standard world model uses an encoder-decoder structure with a data-driven predictor (e.g., LSTM) to model latent dynamics, where the latent representations lack physical meaning. (Right) The PIWM architecture learns a structured latent representation  $z^*$  from images, uses a learnable dynamics model  $\phi$  with physical priors to predict future latent states, and decodes them into future images.**

supervision samples are drawn. In practice, we synthesize biased supervision noise to satisfy this assumption in Section 4.1.

*Other assumptions.* Our method is designed under several standard and widely adopted assumptions for image-based CPS. First, we assume partial observability from images: the subset of physical variables we aim to recover is identifiable from a sequence of visual observations. Second, we adopt the Markovian system assumption, consistent with most world-model and control formulations: the next state depends only on the current state and action. Third, we assume that a partially known dynamics model provides a reasonable approximation of reality, but does not need to be exact.

### 3 Architecture

We introduce the *Physically Interpretable World Model*, a flexible prediction architecture with physically-grounded representations of high-dimensional observations. It consists of two core components: (1) a physically interpretable autoencoder responsible for learning the state representation, and (2) a learnable dynamics model that predicts the evolution of this representation. A high-level overview of the proposed PIWM architecture is shown in Fig. 2, which contrasts it with a standard world model and highlights the structured, interpretable latent state.

In our formulation, physical interpretability has two components. First, the learned physical latent variables  $z^*$  correspond to meaningful physical quantities such as position, velocity, or other environment-specific state variables  $x$ . Second, the dynamics model  $\phi$  learns to follow physically grounded evolution, ensuring that the temporal behavior of  $z^*$  aligns with the underlying laws of motion. Our goal is to achieve both forms of interpretability directly from high-dimensional image observations under weak supervision.

#### 3.1 Learning Interpretable Representations

The primary goal of the autoencoder is to map a high-dimensional observation  $y$  to a low-dimensional interpretable latent state  $z^*$ .

This representation must be explicitly aligned with the true physical state  $x$ . Per Section 2, we cannot access  $x$  or the analytical form of its supervisory distribution  $p(x)$ . Instead, we are given access to a set of  $L$  state proxy samples,  $\Xi = \{\xi^{(l)}\}_{l=1}^L$ , drawn from  $p(x)$ . To leverage these proxy samples  $\Xi$  for training, we formulate a general interpretability loss,  $\mathcal{L}_{\text{interp}}$ , which measures the discrepancy between a predicted physically interpretable state  $z_p^*$  and the sample set  $\Xi$ . In our experiments, we primarily use a Mean Squared Error (MSE) formulation that penalizes the distance to the empirical mean of the samples:

$$\mathcal{L}_{\text{interp}}(z_p^*, \Xi) = \|z_p^* - \hat{\mu}_\xi\|_2^2, \quad \text{where} \quad \hat{\mu}_\xi = \frac{1}{L} \sum_{l=1}^L \xi^{(l)}. \quad (4)$$

An alternative could be to use the Kullback-Leibler (KL) Divergence against a Gaussian fitted to the samples. This serves as the mechanism for enforcing physical grounding throughout our models.

A central design question in learning representation  $z^*$  is how to manage two competing objectives: reconstructing high-dimensional observations versus aligning the latent space with low-dimensional physical states. We consider two approaches, previously highlighted in Fig. 1. The *Intrinsic* approach attempts to achieve both objectives simultaneously with a single, end-to-end encoder. While potentially more efficient, this forces one network to both capture fine-grained visual details (for reconstruction) and ignore those same details to extract the underlying physical state — a difficult learning task. In contrast, the *Extrinsic* approach follows a two-stage process: a vision autoencoder first learns an intermediate representation focused on reconstruction, and then a second, physical encoder extracts the interpretable state from it. This modularity may stabilize training but risks information loss in the intermediate step. Given the fundamental trade-offs, we will systematically investigate both approaches.

Orthogonal to this architectural choice, a second key design decision is the nature of the latent space  $Z^*$ . *Continuous spaces* can represent high-fidelity physical quantities but lack a built-in

organizational prior, requiring explicit regularization for disentanglement. Conversely, *discrete spaces* enforce regularity by design through their finite codebook but lose precision due to quantization error. Below, we detail the combinations of intrinsic/extrinsic and continuous/discrete approaches.

**3.1.1 Intrinsic Autoencoding.** This approach employs a single, end-to-end encoder  $\mathcal{E} : Y \rightarrow Z^*$  that directly maps an observation  $y$  to the final interpretable latent state  $z^*$ . This unified representation must disentangle visual features from physical semantics, a known challenge where information may leak between different physical attributes and hinder the desired learning [44]. For the case of *continuous* latent space, the encoder outputs the parameters for a posterior distribution  $q(z^* | y)$  over the latent space  $Z^*$ . Sampled from this distribution, a latent vector is then partitioned in a fixed manner:  $z^* = [z_p^*, z_v^*]$ , where  $z_p^*$  is the physically interpretable part and  $z_v^*$  captures the remaining visual information necessary for reconstruction. The full objective follows the  $\beta$ -VAE formulation, with the interpretability loss applied only to  $z_p^*$  and KL loss applied to  $z_v^*$ :

$$\mathcal{L}_{\text{intrinsic-cont}} = \mathcal{L}_{\text{recon}}(y, \hat{y}) + \lambda_{\text{interp}} \mathcal{L}_{\text{interp}}(z_p^*, \Xi) + \beta D_{\text{KL}}(q(z_v^* | y) \| \mathcal{N}(0, I)) \quad (5)$$

For the case of *discrete* latent space, we structure the codebook to be interpretable. Each vector  $e_k$  is partitioned as  $e_k = [e_k^p, e_k^v]$ . Only the visual part  $e_k^v$  is a typical learnable VQ-VAE codebook vector. The physical part  $e_k^p$  is a constant vector representing a specific point in a discretized grid of physical values (e.g., specific positions). Then, the interpretable state is computed as the average of the physical portions of the codebook vectors,  $z_p^* = \frac{1}{|I|} \sum_{i \in I} e_i^p$ . The full objective combines the standard VQ loss with our interpretability loss:

$$\mathcal{L}_{\text{intrinsic-disc}} = \mathcal{L}_{\text{VQ}}(y, \hat{y}) + \lambda_{\text{interp}} \mathcal{L}_{\text{interp}}(z_p^*, \Xi), \quad (6)$$

where  $\mathcal{L}_{\text{VQ}}$  includes reconstruction, codebook, and commitment losses:

$$\mathcal{L}_{\text{VQ}} = \|y - \hat{y}\|_2^2 + \|\text{sg}[z_{\text{cont}}] - z_q\|_2^2 + \beta \|z_{\text{cont}} - \text{sg}[z_q]\|_2^2 \quad (7)$$

Here,  $z_{\text{cont}}$  is the continuous output of the encoder  $\mathcal{E}$ , and  $z_q$  is its nearest vector from the codebook. The  $\text{sg}[\cdot]$  is the stop-gradient operator, which ensures that gradients are routed correctly for the codebook loss (updating  $z_q$ ) and the commitment loss (updating  $z_{\text{cont}}$ ). The hyperparameter  $\beta$  weights this commitment loss, controlling how strongly the encoder’s output is encouraged to match the chosen codebook vector.

**3.1.2 Extrinsic Autoencoding.** This approach utilizes a two-stage training process to decouple perception from interpretation. First, a general-purpose vision autoencoder ( $\mathcal{E}_v, \mathcal{D}_v$ ) is trained to map an observation  $y$  to an intermediate latent vector  $z = \mathcal{E}_v(y)$ . This stage is trained with a standard objective, independent of physical supervision. For the *continuous* case, this is a  $\beta$ -VAE trained to minimize:

$$\mathcal{L}_{\text{vision-cont}} = \mathcal{L}_{\text{recon}}(y, \hat{y}) + \beta D_{\text{KL}}(q(z | y) \| \mathcal{N}(0, I)) \quad (8)$$

For the *discrete* case, a VQ-VAE is trained to minimize the standard VQ loss  $\mathcal{L}_{\text{vision-disc}} = \mathcal{L}_{\text{VQ}}(y, \hat{y})$ .

After the first stage, the vision encoder  $\mathcal{E}_v$  is frozen. The second stage trains a separate, auxiliary physical autoencoder ( $\mathcal{E}_p, \mathcal{D}_p$ ) to map the intermediate representation  $z = \mathcal{E}_v(y)$  to a final, purely

physical representation  $z^* = \mathcal{E}_p(z)$ . The training objective for this stage is:

$$\mathcal{L}_{\text{physical}} = \lambda_{\text{interp}} \mathcal{L}_{\text{interp}}(z^*, \Xi) + \lambda_{\text{latent}} \mathcal{L}_{\text{recon}}(z, \mathcal{D}_p(z^*)) \quad (9)$$

This same loss  $\mathcal{L}_{\text{physical}}$  is used for both continuous and discrete intermediate representation  $z$ . Additional architectural diagrams of the extrinsic–discrete pipeline are provided in the Appendix (Figure 7) for clarity.

## 3.2 Learnable Dynamics Model

The second core component of our PIWM is a latent dynamics model  $\phi$  that predicts the temporal evolution of the physically interpretable state  $z^*$ . Rather than using black-box sequence models, our prediction is based on known dynamics equations,  $\phi(z_t^*, a_t, \theta)$ , where the form of  $\phi$  (e.g., kinematics) is fixed and only its parameters  $\theta$  are learnable. This allows our model to reflect the underlying physical laws while adapting to unknown system parameters  $\theta$  such as friction and mass.

The dynamics model is responsible for estimating physical quantities that depend on a history of states, such as velocity, in order to predict the system’s evolution. To do this, the model is initialized with a short window of consecutive representations,  $(z_t^*, z_{t+1}^*)$ , produced by the encoder from observations. These two states, along with the control action  $a_{t+1}$  that causes the transition from state  $t + 1$  to  $t + 2$ , are used by the learnable dynamics model  $\phi$  to predict the next state:  $\hat{z}_{t+2}^* = \phi(z_t^*, z_{t+1}^*, a_{t+1}, \theta)$ . By taking two consecutive states as input, the model can internally compute velocity and other time-derivative quantities necessary for an accurate physical prediction. This method can be extended to higher-order derivatives with more consecutive inputs. After this initialization phase, the model can operate recursively for multi-step rollouts, taking its own prediction from the previous step as input to generate a future trajectory. This enables efficient, long-horizon forecasting without needing a sequence of observations at every step.

The parameters  $\theta$  of the dynamics model  $\phi$  are learned by minimizing a dynamics loss,  $\mathcal{L}_{\text{dyn}}$ . This objective ensures that the predicted state  $\hat{z}_{t+H}^*$ , generated by recursively applying the dynamics model  $\phi(\cdot, \cdot, \theta)$ , aligns with the weak supervision available for that future time step. We use a Mean Squared Error (MSE) loss, which compares the prediction against the empirical mean of the proxy labels  $\Xi_{t+H}$ . The loss is defined as a function of the parameters  $\theta$ :

$$\mathcal{L}_{\text{dyn}}(\theta) = \|\hat{z}_{t+H}^* - \hat{\mu}_{\xi_{t+H}}\|_2^2, \quad (10)$$

where  $\hat{z}_{t+H}^*$  is the state predicted by the dynamics model parameterized by  $\theta$ , and  $\hat{\mu}_{\xi_{t+H}} = \frac{1}{L} \sum_{l=1}^L \xi_{t+H}^{(l)}$  is the empirical mean of the  $L$  proxy samples for the future state.

To optimize the learnable parameters  $\theta$ , we backpropagate through the structured *second-order* dynamics model used in Algorithm 1. Since each predicted state  $\hat{z}_{t+H}^*$  is obtained by recursively applying

$$\hat{z}_{t+2}^* = \phi(z_t^*, z_{t+1}^*, a_{t+1}; \theta), \quad (11)$$

it depends on *two* previous latent states, consistent with the model definition. The gradient of the multi-step dynamics loss is:

$$\frac{\partial \mathcal{L}_{\text{dyn}}}{\partial \theta} = \frac{\partial \mathcal{L}_{\text{dyn}}}{\partial \hat{z}_{t+H}^*} \cdot \frac{\partial \hat{z}_{t+H}^*}{\partial \theta}. \quad (12)$$

**Algorithm 1** Training pipeline for PIWM. Models are trained in separate stages, freezing the parameters of earlier stages before optimizing the next one.

---

**Input:** Training set  $\mathcal{S}$ , batch size  $B$ , weights  $\{\lambda_i\}$

```

1: // Stage 1: Train the vision autoencoder (extrinsic only)
2: if architecture = extrinsic then
3:   for epoch = 1 to  $n_{\text{vision}}$  do
4:     for each batch of  $(y_t)$  do
5:        $z_t \leftarrow \mathcal{E}_v(y_t)$ 
6:       if latent = discrete then
7:          $z_t \leftarrow \text{Quantize}(z_t)$ 
8:       end if
9:        $\hat{y}_t \leftarrow \mathcal{D}_v(z_t)$ 
10:       $\mathcal{L}_{\text{vision}} \leftarrow \mathcal{L}_{\text{rec}}(y_t, \hat{y}_t) + \lambda_3 \mathcal{L}_{\text{reg}}$ 
11:      Update  $(\mathcal{E}_v, \mathcal{D}_v)$  using  $\nabla \mathcal{L}_{\text{vision}}$ 
12:    end for
13:  end for
14:  Freeze parameters of  $\mathcal{E}_v$ 
15: end if
16: // Stage 2: Train the physical encoder–decoder
17: for epoch = 1 to  $n_{\text{physical}}$  do
18:   for each batch of  $(y_t, \Xi_t)$  do
19:     if architecture = intrinsic then
20:        $z_t^* \leftarrow \mathcal{E}(y_t)$ 
21:     else
22:        $z_t \leftarrow \mathcal{E}_v(y_t)$ 
23:       if latent = discrete then
24:          $z_t \leftarrow \text{Quantize}(z_t)$ 
25:       end if
26:        $z_t^* \leftarrow \mathcal{E}_p(z_t)$ 
27:     end if
28:     Compute interpretability loss  $\mathcal{L}_{\text{interp}}(z_t^*, \Xi_t)$ 
29:     if architecture = extrinsic then
30:        $\hat{z}_t \leftarrow \mathcal{D}_p(z_t^*)$ 
31:        $\mathcal{L}_{\text{latent-rec}} \leftarrow \|z_t - \hat{z}_t\|^2$ 
32:     else
33:        $\mathcal{L}_{\text{latent-rec}} \leftarrow 0$ 
34:     end if
35:      $\mathcal{L}_{\text{phys}} \leftarrow \lambda_1 \mathcal{L}_{\text{interp}} + \lambda_2 \mathcal{L}_{\text{latent-rec}}$ 
36:     Update physical encoder–decoder using  $\nabla \mathcal{L}_{\text{phys}}$ 
37:   end for
38: end for
39: Freeze  $\mathcal{E}$  (intrinsic) or  $(\mathcal{E}_p, \mathcal{D}_p)$  (extrinsic)
40: // Stage 3: Train the dynamics model
41: for epoch = 1 to  $n_{\text{dyn}}$  do
42:   for each batch of  $(y_{t:t+2}, a_t, \Xi_{t:t+2})$  do
43:     Encode states to obtain  $z_t^*, z_{t+1}^*$ 
44:     Predict next physical state  $\hat{z}_{t+2}^* \leftarrow \phi_\theta(z_t^*, z_{t+1}^*, a_t)$ 
45:     Compute dynamics loss  $\mathcal{L}_{\text{dyn}}(\hat{z}_{t+2}^*, \Xi_{t+2})$ 
46:     Update  $\theta$  using  $\nabla \mathcal{L}_{\text{dyn}}$ 
47:   end for
48: end for
49: return trained model parameters

```

---

The recursive derivative for  $\hat{z}_{t+H}^*$  expands as:

$$\frac{\partial \hat{z}_{t+H}^*}{\partial \theta} = \frac{\partial \phi}{\partial \theta} + \frac{\partial \phi}{\partial z_{t+H-1}^*} \cdot \frac{\partial z_{t+H-1}^*}{\partial \theta} + \frac{\partial \phi}{\partial z_{t+H-2}^*} \cdot \frac{\partial z_{t+H-2}^*}{\partial \theta}, \quad (13)$$

reflecting the fact that the dynamics model  $\phi$  takes

$$(z_{t+H-2}^*, z_{t+H-1}^*, a_{t+H-1})$$

as inputs. This recursive computation enables end-to-end learning of both the interpretable latent states and the dynamics parameters, ensuring that the learned physical parameters remain consistent with observed trajectories. During training, the dynamics model is optimized after the representation modules have been trained and frozen.

### 3.3 Training Procedure

PIWM is not trained end-to-end for all variants. Intrinsic and models are trained in two and three stages: the vision autoencoder is trained first and then frozen; the physical encoder–decoder is trained next and then frozen (only for extrinsic one); finally, the dynamics model is trained with both encoders fixed. Algorithm 1 illustrates the unified forward pass, while the actual optimization for extrinsic models follows this staged schedule. Algorithm 1 therefore describes a conceptual per-timestep update, while the actual optimization is performed using this staged schedule. Algorithm 1 summarizes our unified training framework for PIWM, which integrates the learning of interpretable representations with dynamics modeling. The training operates on a dataset

$$\mathcal{S} = \{(y_{1:M}, a_{1:M}, \Xi_{1:M})\}_{i=1}^N,$$

consisting of  $N$  trajectories, where each trajectory contains  $M$  time steps of observations  $y$ , actions  $a$ , and weak supervision samples  $\Xi$ . The model parameters  $w$  are optimized using mini-batch gradient descent with batch size  $B$  and learning rate  $\eta$  over  $n_{\text{epochs}}$  epochs.

The training follows a four-stage process within each time step: **Stage 1: Encoding.** For intrinsic architectures, observations are directly encoded to interpretable states  $z^*$  via encoder  $\mathcal{E}$ . For extrinsic architectures, a two-stage process first encodes observations to intermediate representations  $z$  using vision encoder  $\mathcal{E}_v$ , then maps them to physical states  $z_p^*$  via physical encoder  $\mathcal{E}_p$ . Discrete variants apply quantization after encoding.

**Stage 2: Dynamics Prediction.** The learnable dynamics model  $\phi_\theta$  takes two consecutive physical states  $z_p^*[t], z_p^*[t+1]$  and action  $a_t = h(y_t)$  from controller  $h$  to predict the next state  $\hat{z}_p^*[t+2]$ . This enables the model to internally compute velocities and other derivatives necessary for physical prediction.

**Stage 3: Decoding.** Intrinsic models decode by combining predicted physical states with visual features. Extrinsic models first decode to intermediate representations via  $\mathcal{D}_p$ , then to observations via  $\mathcal{D}_v$ .

The total loss combines reconstruction error  $\mathcal{L}_{\text{rec}}$ , interpretability alignment  $\mathcal{L}_{\text{interp}}$  with weak supervision  $\Xi$ , dynamics prediction accuracy  $\mathcal{L}_{\text{dyn}}$ , and regularization  $\mathcal{L}_{\text{reg}}$  (KL divergence for continuous, VQ losses for discrete). Only the relevant components of the loss are active in each training stage.

The key distinction from standard world models lies in the explicit alignment of latent representations with physical quantities through weak supervision and physical priors, to support both accurate prediction and physical interpretability.

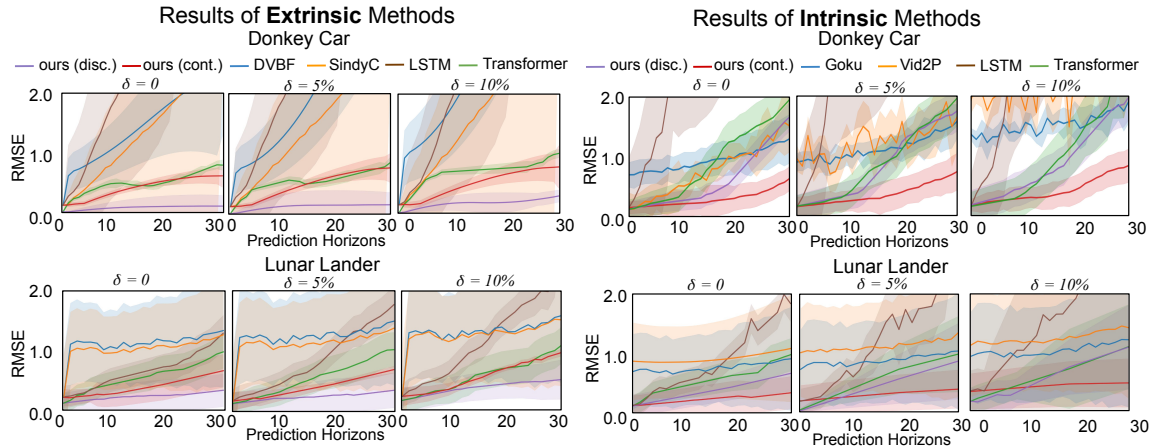


**Figure 3: Prediction performance.** The Root Mean Square Error (RMSE) of our PIWM variants (extrinsic methods, left; intrinsic methods, right) is compared against baselines over a 30-step prediction horizon in the Donkey Car and Lunar Lander across varying levels of weak supervision ( $\delta$ ).

## 4 Experimental Evaluation

To validate our PIWM approach, we experiment on three environments: CartPole, Lunar Lander, and the DonkeyCar autonomous racing platform [5, 54]. These environments differ in the observation dimensionality, action space, and underlying dynamics.

### 4.1 Experimental Setup

For each environment, we collect a dataset of 60,000 trajectories, each with at least 50 time steps. To ensure diverse state space coverage, trajectories are generated by executing both random actions and those generated by well-trained neural controllers.

The weak supervision labels used in all experiments instantiate the uniform-distribution noise model described in Sec. 2. In practice, this means that the supervisory distribution  $p(x)$  for each state dimension is implemented as a biased uniform distribution over a bounded interval of relative width  $\delta$ . For each ground-truth state component  $x_i$ , let  $\mathcal{X}_i$  denote the valid range size of that dimension. We first generate a randomly shifted center:

$$\tilde{\mu}_i = x_i + \Delta_i, \quad \Delta_i \sim \text{Unif}\left[-\frac{1}{2}\delta |\mathcal{X}_i|, \frac{1}{2}\delta |\mathcal{X}_i|\right].$$

We then define the supervisory distribution itself as a uniform distribution supported on an interval of the same width:

$$p_i(x) = \text{Unif}\left[\tilde{\mu}_i - \frac{1}{2}\delta |\mathcal{X}_i|, \tilde{\mu}_i + \frac{1}{2}\delta |\mathcal{X}_i|\right].$$

At each time step, we draw 50 samples from this distribution to form the proxy supervision set  $\Xi$  used in training.

For the experiments, our vision encoder  $\mathcal{E}_v$  uses two convolutional layers with channel projection to a 64-dimensional latent space. Discrete variants employ a 512-entry codebook with commitment loss weight  $\beta = 0.25$ . The physical encoder  $\mathcal{E}_p$  is a 2-layer Transformer (4 heads, 512 feedforward dimension) with mean pooling and linear projection to physical states. The decoder  $\mathcal{D}_p$  mirrors this architecture. We apply early stopping based on validation loss to prevent overfitting and to ensure stable convergence across environments. In addition, we use a cosine learning-rate decay schedule, which improves long-horizon rollout stability for the second-order

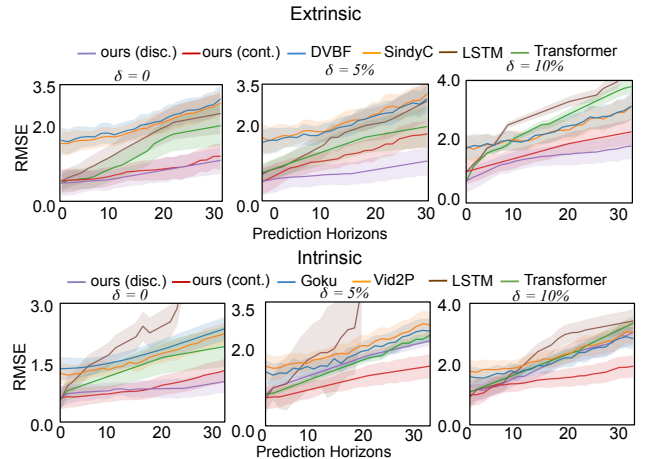


**Figure 4: Prediction performance of CartPole.** The Root Mean Square Error (RMSE) of our PIWM variants (extrinsic methods, upper; intrinsic methods, lower) is compared against baselines over a 30-step prediction horizon in the CartPole across varying levels of weak supervision ( $\delta$ ).

latent dynamics model. These training settings follow standard practices in world-model and VQ-VAE training. We performed a small-scale sweep over candidate learning rates and regularization magnitudes and selected the configuration that yielded stable reconstruction loss, non-diverging rollouts, and consistent convergence across datasets. More details can be found in the Appendix.

We evaluate our PIWM variants (Intrinsic/Extrinsic, Continuous/Discrete) against a suite of strong baselines under 5-fold cross-validation. We first include data-driven sequence models, an *LSTM* and a *Transformer*, which serve as non-physical benchmarks. Our primary comparisons are to state-of-the-art models in two categories. For the intrinsic approach, we compare against *Vid2Para* [2]

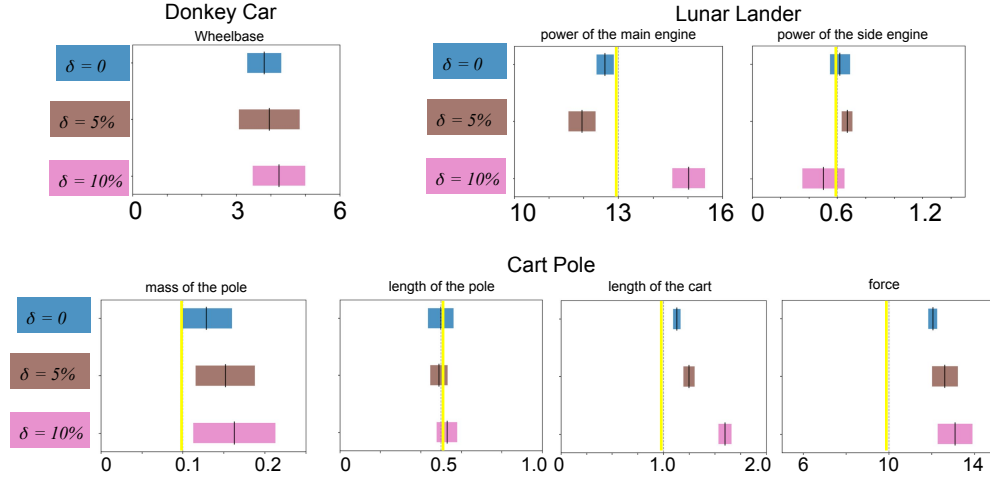


**Figure 5: Learned physical parameters vs. ground truth. For Cart Pole and Lunar Lander, the parameters learned by our model (colored bars) are compared against the known ground-truth values (yellow lines) under varying noise levels ( $\delta$ ). For the Donkey Car, we use only an approximate bicycle model and the true physical parameters are unknown; therefore, no ground-truth reference is shown.**

and *GokuNet* [35]. For the extrinsic approach, we evaluate against *DVBF* [24]. To specifically isolate and compare the performance of the latent dynamics predictors, we also include *SindyC* [6] — a classic state-based method for dynamics discovery. For a fair comparison, both the *DVBF* and *SindyC* dynamics models operate on the interpretable latent representations produced by our continuous autoencoder. All models are configured to have a comparable parameter count to focus the comparison on architectural efficacy rather than model capacity. The controller used in all experiments is pretrained and kept fixed throughout the training of PIWM. It is not jointly optimized with the image encoder, the physical encoder, or the dynamics model. Instead, it is trained separately using ground-truth states under a standard supervised imitation-learning objective. During PIWM training, the controller serves only as an action generator, and its parameters remain frozen so that the learning of the latent physical representations and dynamics is not influenced by updates to the control policy.

## 4.2 Predictive Performance

*Extrinsic vs. intrinsic performance.* We first evaluate the primary task of long-horizon trajectory prediction. Figure 3 shows the root mean square error (RMSE) for 30-step future state prediction in the challenging Donkey Car environment, comparing both extrinsic and intrinsic methods across different levels of supervision noise,  $\delta$ . The results for extrinsic methods (Fig. 3) show a clear performance hierarchy. Our PIWM variants consistently outperform all baselines. The quantized extrinsic model (purple line) achieves the lowest and most stable prediction error, maintaining accuracy even as the prediction horizon extends. Our continuous extrinsic model (red line) is the second-best performer. Both significantly surpass the extrinsic baselines (*DVBF*, *SindyC*) and the purely data-driven models (LSTM, Transformer), whose errors escalate rapidly.

A more nuanced picture emerges for the intrinsic methods (Fig. 3, right). Our PIWM models again demonstrate a clear advantage over the *Vid2Para* and *GokuNet* baselines. Strikingly, our continuous intrinsic model (red line) achieves a predictive accuracy that is highly competitive with, and in some cases even surpasses, our top-performing extrinsic models. This suggests that a well-regularized, end-to-end continuous architecture can be highly effective. In contrast, the quantized intrinsic model (purple line) exhibits less stability and higher error in this configuration, indicating that the optimization challenge of aligning a discrete codebook within a single, unified encoder is considerable. Nevertheless, both of our intrinsic variants outperform the baseline models, confirming the overall benefit of our training methodology.

*Continuous vs. discrete latent spaces.* A key insight from these results is that decoupling visual perception from physical state inference (the extrinsic approach) is a critical design choice for achieving robust, long-term prediction. An important observation from our results is the different strengths exhibited by continuous and discrete latent parameterizations across the intrinsic and extrinsic settings. In the intrinsic (one-stage) architecture, the encoder must jointly learn visual abstractions and physically structured representations. This joint optimization benefits from the flexibility and smooth gradients of a continuous latent space, which can more easily adapt to the coupled visual-physical objectives. In contrast, the extrinsic (two-stage) architecture decouples visual encoding from physical interpretation. In this setting, the discrete latent space acts as a strong regularizer: the quantization suppresses visual noise, stabilizes the mapping to physical states, and improves generalization of the dynamics model. Consequently, the continuous variant performs better under the intrinsic setup, while the discrete variant achieves superior performance under the extrinsic setup.

*Takeaway:* the optimal latent parameterization depends on whether physical structure is learned jointly with perception or inferred

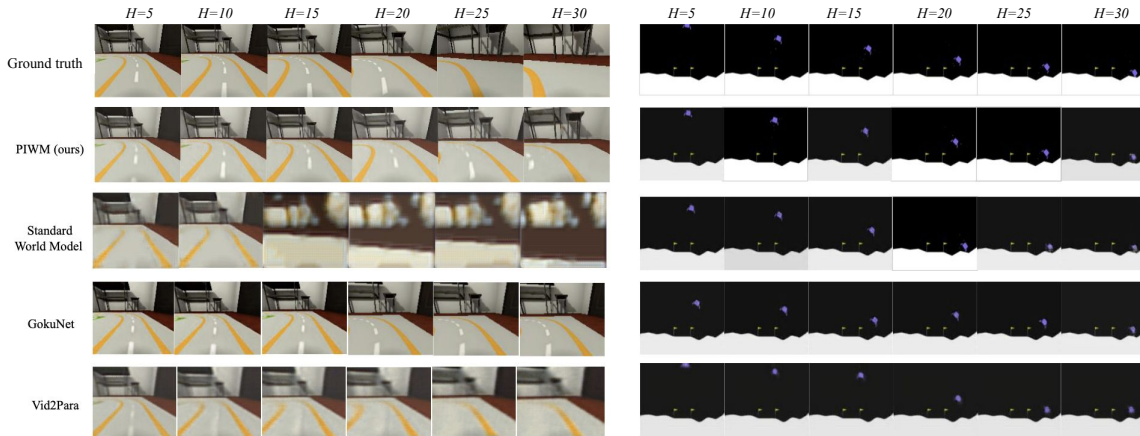


Figure 6: Qualitative comparison of 30-step trajectory rollouts under  $\delta = 5\%$ .

from a pre-learned visual representation. Furthermore, across both architectures, the quantized (discrete) latent space provides a powerful regularization effect, leading to more stable predictions than the continuous alternative, especially under noisy supervision.

### 4.3 Physicality of Learned Representations

Strong predictive performance should stem from accurate underlying states and dynamics. We validate this by evaluating the static encoding quality and the model’s ability to recover the true physical parameters of the simulation.

Table 1 presents the static encoding RMSE, measuring how accurately each model can infer the physical state from a single observation. The results strongly correlate with the predictive findings. Our quantized extrinsic PIWM achieves the highest encoding accuracy, confirming that its superior representation is the foundation of its predictive power. The intrinsic continuous models, while competitive, exhibit higher encoding error, consistent with their weaker predictive performance.

Finally, we assess whether the dynamics model can learn the true physical parameters (e.g., car length, pole mass) within the learned latent space. As reported in Figure 5, PIWM successfully recovers the ground-truth parameters with low relative error across all environments. This provides direct evidence that our framework learns a genuinely interpretable representation that is not merely correlated with the physics — but is structured in a physically grounded way.

## 5 Analysis and Discussion

Our experiment demonstrates that the extrinsic architecture with a discrete latent space is optimal for learning physically interpretable world models from weak supervision. This approach achieves superior prediction accuracy (Figure 3) by decoupling perception from physical state abstraction and leveraging quantization as a powerful regularizer against visual noise. The learned representations are not only predictive but also genuinely physically grounded, as evidenced by the model’s ability to recover true system parameters (Figure 5) and generate qualitatively plausible visual rollouts

that far exceed baseline performance (Figure 6). Crucially, the substantial gains in interpretability and prediction accuracy come at a minimal cost to downstream controller performance (Table 2), validating our architecture as a robust and practical solution. DVBF performs poorly in our settings because its Gaussian latent space and amortized inference provide no physical inductive bias, causing the learned states to drift and quickly accumulate errors during multi-step rollouts. This makes DVBF unstable in visually rich or discontinuous dynamics environments, which explains its large performance gap relative to structured models such as PIWM.

While our framework is effective, future work should focus on scaling its representational capacity and enhancing its use of supervision. For complex, open-world scenarios like autonomous driving, our approach could be extended from predicting simple state vectors to building structured world representations, such as dynamic 3D occupancy grids, where physical priors can be applied to multiple agents. Furthermore, the rich temporal nature of weak supervision signals is currently underutilized. Future methods could process sequences of noisy supervisory signals using filtering or sequence modeling techniques to produce a more refined, temporally coherent learning target, thereby improving the model’s robustness and accuracy. Also, the experiments in this work focus on Markovian dynamical systems, where transitions depend only on the most recent latent state and action. This setting aligns with the majority of prior work on world models and enables a clean evaluation of the proposed physically interpretable latent dynamics. Extending PIWM to non-Markovian or delayed-effect systems, where temporal dependencies span multiple steps, represents an interesting direction for future research. Evaluating such scenarios would require augmenting the dynamics model with additional memory mechanisms or explicitly modeling higher-order temporal dependencies.

## 6 Related Work

### 6.1 Trajectory Prediction

Predicting trajectories is critical for safe planning and control [13], but existing methods present trade-offs. While approaches like

**Table 1: Static state encoding error under weak supervision. For each environment and model variant, we report the mean  $\pm$  std of (1) MSE between the predicted static latent  $z_p^*$  and the empirical mean of the weak-supervision samples, and (2) KL divergence for continuous variants. Columns correspond to different supervision noise levels  $\delta$ . Lower values indicate better alignment between latent representations and static physical state variables (e.g., position, angle).**

Case	Model	$\delta = 0\%$		$\delta = 5\%$		$\delta = 10\%$	
		MSE	KL	MSE	KL	MSE	KL
Donkey Car	Intrinsic (Cont.)	0.13 $\pm$ 0.05	0.45 $\pm$ 0.06	0.16 $\pm$ 0.06	0.52 $\pm$ 0.07	0.20 $\pm$ 0.07	0.58 $\pm$ 0.08
	Intrinsic (Disc.)	0.18 $\pm$ 0.04	0.42 $\pm$ 0.05	0.21 $\pm$ 0.05	0.55 $\pm$ 0.06	0.22 $\pm$ 0.06	0.64 $\pm$ 0.07
	Extrinsic (Cont.)	0.11 $\pm$ 0.05	0.24 $\pm$ 0.04	0.15 $\pm$ 0.04	0.28 $\pm$ 0.05	0.16 $\pm$ 0.05	0.33 $\pm$ 0.06
	<b>Extrinsic (Disc.)</b>	0.03 $\pm$ 0.02	0.19 $\pm$ 0.03	0.05 $\pm$ 0.03	0.23 $\pm$ 0.04	0.06 $\pm$ 0.04	0.28 $\pm$ 0.05
Lunar Lander	Intrinsic (Cont.)	0.07 $\pm$ 0.05	0.56 $\pm$ 0.26	0.08 $\pm$ 0.15	0.58 $\pm$ 0.37	0.21 $\pm$ 0.07	0.77 $\pm$ 0.38
	Intrinsic (Disc.)	0.06 $\pm$ 0.04	0.44 $\pm$ 0.11	0.03 $\pm$ 0.05	0.53 $\pm$ 0.12	0.16 $\pm$ 0.06	0.64 $\pm$ 0.17
	Extrinsic (Cont.)	0.11 $\pm$ 0.07	0.33 $\pm$ 0.14	0.14 $\pm$ 0.04	0.39 $\pm$ 0.16	0.15 $\pm$ 0.05	0.45 $\pm$ 0.26
	<b>Extrinsic (Disc.)</b>	0.03 $\pm$ 0.02	0.24 $\pm$ 0.14	0.09 $\pm$ 0.03	0.29 $\pm$ 0.11	0.12 $\pm$ 0.04	0.35 $\pm$ 0.23

Hamilton-Jacobi (HJ) reachability offer formal guarantees [31, 42], they are computationally expensive for online settings. Conversely, mainstream deep learning models are powerful but often rely on handcrafted scene representations [47] or high-precision maps [20, 22], and typically do not produce physically interpretable predictions [34, 36, 46]. In contrast, our approach learns directly from raw images with distribution-based weak supervision without requiring handcrafted inputs or goal conditioning.

## 6.2 Representation Learning

A central challenge in learning from high-dimensional sequences is creating compact and meaningful latent representations [3, 50]. While Variational Autoencoders (VAEs) [27] are foundational, their standard form learns unstructured latents. A significant line of research attempts to impose structure, either by encouraging disentanglement in continuous spaces with methods like  $\beta$ -VAE, FactorVAE, and TCVAE [8, 19, 26], or by enforcing causality [60]. However, these methods often fall short of ensuring a direct correspondence with real-world physical states or require precisely labeled data. An alternative is to impose structure via discretization with Vector-Quantized VAEs (VQ-VAEs) and their extensions [45, 53, 58]. While effective, their application to physical prediction has been limited due to abstract latent codes and reliance on exact supervision. Even in robotic applications like DVQ-VAE that model structured systems, encoding external environmental factors remains a challenge [62]. GOKU-net constrains variables to plausible physical ranges but does not tie them to specific, interpretable quantities [35].

Other works incorporate structured priors to enhance learning. Object-centric world models like FOCUS [12] and foundation world models [38] improve efficiency by structuring latents around discrete entities. Models like SPARTAN [30] provide outputs that are interpretable by construction but do not incorporate known physical dynamics or action-conditioned prediction. Priors can also be introduced as task-related rules in Bayesian neural networks [48] or through human and self-supervision to guide abstraction [7, 14, 28, 43, 56]. These approaches, however, often yield abstract representations that lack physical grounding without strong external priors. Closer to our work, Deep Variational Bayes Filters (DVBFs) extend VAEs with a latent dynamics module [24]. Yet, without explicit physical supervision, they often fail to recover

interpretable variables — a limitation our work addresses by leveraging weak supervision.

## 6.3 World Models

Classical world models like Dreamer [16] and DayDreamer [57] excel at learning from experience for policy learning, but their latent representations are typically uninterpretable [44]. Many approaches seek to improve physical grounding by incorporating priors, such as bounds on states and actions [51, 52], physics-aware loss functions [11], or kinematics-inspired layers [9]. However, these methods are often designed for low-dimensional systems and do not scale well to learning from noisy, high-dimensional images. Other physics-informed methods leverage differential equations to stabilize learning [35, 64], with frameworks like Phy-Taylor using Taylor monomials to structure the latent dynamics [37]. Approaches like sparse identification and differentiable physics require access to the underlying state variables and are not designed to learn from raw visual inputs [6, 10, 61].

Recent advances have produced powerful but distinct world models. For instance, 3D occupancy-based models improve forecasting but their internal states are not explicitly aligned with physical variables [40, 59, 63, 65]. Concurrently, neuro-symbolic models enhance generalization but require predefined symbolic inputs not available from raw sensor data [4, 32]. Our approach is distinct from these paradigms as it learns physically interpretable representations directly from images using weak supervision. This also contrasts with the most closely related work, Vid2Param [2], which requires full supervision and struggles with dynamics prediction.

## 7 Conclusion

We presented the Physically Interpretable World Model, a framework that learns physically-grounded latent representations from images using only weak distributional supervision. Our systematic evaluation demonstrates that an extrinsic architecture with a discrete latent space yields accurate and robust predictions and successfully recovers the system’s true physical parameters. This work not only provides direct evidence of a physically interpretable model — but also offers a practical path toward more trustworthy and reliable cyber-physical systems with generative predictors.

## References

- [1] Mohammed Alshiekh, Roderick Bloem, Rüdiger Ehlers, Bettina Könighofer, Scott Niekum, and Ufuk Topcu. 2018. Safe reinforcement learning via shielding. In *Proceedings of the AAAI conference on artificial intelligence*, Vol. 32.
- [2] Martin Asenov, Michael Burke, Daniel Angelov, Todor Davchev, Kartic Subr, and Subramanian Ramamoorthy. 2019. Vid2param: Modeling of dynamics parameters from video. *IEEE Robotics and Automation Letters* 5, 2 (2019), 414–421.
- [3] Shaojie Bai, J Zico Kolter, and Vladlen Koltun. 2018. An empirical evaluation of generic convolutional and recurrent networks for sequence modeling. *arXiv preprint arXiv:1803.01271* (2018).
- [4] Jonathan Balloch, Zhiyu Lin, Robert Wright, Xiangyu Peng, Mustafa Hussain, Aarun Srinivas, Julia Kim, and Mark O Riedl. 2023. Neuro-symbolic world models for adapting to open world novelty. *arXiv preprint arXiv:2301.06294* (2023).
- [5] Greg Brockman, Vicki Cheung, Ludwig Pettersson, Jonas Schneider, John Schulman, Jie Tang, and Wojciech Zaremba. 2016. Openai gym. *arXiv preprint arXiv:1606.01540* (2016).
- [6] Steven L. Brunton, Joshua L. Proctor, and J. Nathan Kutz. 2016. Sparse Identification of Nonlinear Dynamics with Control (SINDyC). *IFAC-PapersOnLine* 49, 18 (2016), 710–715. doi:10.1016/j.ifacol.2016.10.249 10th IFAC Symposium on Nonlinear Control Systems NOLCOS 2016.
- [7] Boyuan Chen, Kuang Huang, Sunand Raghupathi, Ishaan Chandratreya, Qiang Du, and Hod Lipson. 2022. Automated discovery of fundamental variables hidden in experimental data. *Nature Computational Science* 2, 7 (2022), 433–442.
- [8] Ricky TQ Chen, Xuechen Li, Roger B Grosse, and David K Duvenaud. 2018. Isolating sources of disentanglement in variational autoencoders. *Advances in neural information processing systems* 31 (2018).
- [9] Henggang Cui, Thi Nguyen, Fang-Chieh Chou, Tsung-Han Lin, Jeff Schneider, David Bradley, and Nemanja Djuric. 2020. Deep kinematic models for kinematically feasible vehicle trajectory predictions. In *2020 IEEE International Conference on Robotics and Automation (ICRA)*. IEEE, 10563–10569.
- [10] Filipe de Avila Belbute-Peres, Kevin Smith, Kelsey Allen, Josh Tenenbaum, and J Zico Kolter. 2018. End-to-end differentiable physics for learning and control. *Advances in neural information processing systems* 31 (2018).
- [11] Franck Djeumou, Cyrus Neary, and Ufuk Topcu. 2023. How to learn and generalize from three minutes of data: Physics-constrained and uncertainty-aware neural stochastic differential equations. *arXiv preprint arXiv:2306.06335* (2023).
- [12] Stefano Ferraro, Pietro Mazzaglia, Tim Verbelen, and Bart Dhoedt. 2023. Focus: Object-centric world models for robotics manipulation. *arXiv preprint arXiv:2307.02427* (2023).
- [13] David Fridovich-Keil, Andrea Bajcsy, Jaime F Fisac, Sylvia L Herbert, Steven Wang, Anca D Dragan, and Claire J Tomlin. 2020. Confidence-aware motion prediction for real-time collision avoidance. *The International Journal of Robotics Research* 39, 2-3 (2020), 250–265.
- [14] Xiang Fu, Ge Yang, Pulkit Agrawal, and Tommi Jaakkola. 2021. Learning task informed abstractions. In *International Conference on Machine Learning*. PMLR, 3480–3491.
- [15] David Ha and Jürgen Schmidhuber. 2018. World models. *arXiv preprint arXiv:1803.10122* (2018).
- [16] Danijar Hafner, Timothy Lillicrap, Mohammad Norouzi, and Jimmy Ba. 2020. Mastering atari with discrete world models. *arXiv preprint arXiv:2010.02193* (2020).
- [17] Danijar Hafner, Jurgis Pasukonis, Jimmy Ba, and Timothy Lillicrap. 2023. Mastering diverse domains through world models. *arXiv preprint arXiv:2301.04104* (2023).
- [18] Osman Hasan and Sofiene Tahar. 2015. Formal verification methods. In *Encyclopedia of Information Science and Technology, Third Edition*. IGI global, 7162–7170.
- [19] Irina Higgins, Loic Matthey, Arka Pal, Christopher P Burgess, Xavier Glorot, Matthew M Botvinick, Shakir Mohamed, and Alexander Lerchner. 2017. beta-vae: Learning basic visual concepts with a constrained variational framework. *ICLR (Poster)* 3 (2017).
- [20] Kai-Chieh Hsu, Karen Leung, Yuxiao Chen, Jaime F Fisac, and Marco Pavone. 2023. Interpretable Trajectory Prediction for Autonomous Vehicles via Counterfactual Responsibility. In *2023 IEEE/RSJ International Conference on Intelligent Robots and Systems (IROS)*. IEEE, 5918–5925.
- [21] Ahmed Hussein, Mohamed Medhat Gaber, Eyad Elyan, and Chrisina Jayne. 2017. Imitation learning: A survey of learning methods. *ACM Computing Surveys (CSUR)* 50, 2 (2017), 1–35.
- [22] Masha Itkina and Mykel Kochenderfer. 2023. Interpretable self-aware neural networks for robust trajectory prediction. In *Conference on Robot Learning*. PMLR, 606–617.
- [23] Leslie Pack Kaelbling, Michael L Littman, and Andrew W Moore. 1996. Reinforcement learning: A survey. *Journal of artificial intelligence research* 4 (1996), 237–285.
- [24] Maximilian Karl, Maximilian Soelch, Justin Bayer, and Patrick Van der Smagt. 2016. Deep variational bayes filters: Unsupervised learning of state space models from raw data. *arXiv preprint arXiv:1605.06432* (2016).
- [25] Sydney M Katz, Anthony L Corso, Christopher A Strong, and Mykel J Kochenderfer. 2022. Verification of image-based neural network controllers using generative models. *Journal of Aerospace Information Systems* 19, 9 (2022), 574–584.
- [26] Hyunjik Kim and Andriy Mnih. 2018. Disentangling by factorising. In *International conference on machine learning*. PMLR, 2649–2658.
- [27] Diederik P Kingma. 2013. Auto-encoding variational bayes. *arXiv preprint arXiv:1312.6114* (2013).
- [28] George Konidaris, Leslie Pack Kaelbling, and Tomas Lozano-Perez. 2018. From skills to symbols: Learning symbolic representations for abstract high-level planning. *Journal of Artificial Intelligence Research* 61 (2018), 215–289.
- [29] Long Le, Ryan Lucas, Chen Wang, Chuhao Chen, Dinesh Jayaraman, Eric Eaton, and Lingjie Liu. 2025. Pixie: Fast and Generalizable Supervised Learning of 3D Physics from Pixels. *arXiv preprint arXiv:2508.17437* (2025).
- [30] Anson Lei, Bernhard Schölkopf, and Ingmar Posner. 2024. SPARTAN: A sparse transformer learning local causation. *arXiv preprint arXiv:2411.06890* (2024).
- [31] Anjian Li, Liting Sun, Wei Zhan, Masayoshi Tomizuka, and Mo Chen. 2021. Prediction-based reachability for collision avoidance in autonomous driving. In *2021 Intl. Conf. on Robotics and Automation (ICRA)*.
- [32] Yichao Liang, Nishanth Kumar, Hao Tang, Adrian Weller, Joshua B Tenenbaum, Tom Silver, João F Henriques, and Kevin Ellis. 2024. Visualpredicator: Learning abstract world models with neuro-symbolic predicates for robot planning. *arXiv preprint arXiv:2410.23156* (2024).
- [33] TP Lillicrap. 2015. Continuous control with deep reinforcement learning. *arXiv preprint arXiv:1509.02971* (2015).
- [34] Lars Lindemann, Xin Qin, Jyotirmoy V Deshmukh, and George J Pappas. 2023. Conformal prediction for stl runtime verification. In *Proceedings of the ACM/IEEE 14th International Conference on Cyber-Physical Systems (with CPS-IoT Week 2023)*. 142–153.
- [35] Ori Liniat, Neta Ravid, Danny Eytan, and Uri Shalit. 2021. Generative ODE modeling with known unknowns. In *Proceedings of the Conference on Health, Inference, and Learning (CHIL '21)*. Association for Computing Machinery, New York, NY, USA, 79–94. doi:10.1145/3450439.3451866
- [36] Juanwu Lu, Wei Zhan, Masayoshi Tomizuka, and Yeping Hu. 2024. Towards Generalizable and Interpretable Motion Prediction: A Deep Variational Bayes Approach. In *International Conference on Artificial Intelligence and Statistics*. PMLR, 4717–4725.
- [37] Yanbing Mao, Yuliang Gu, Lui Sha, Huajie Shao, Qixun Wang, and Tarek Abdelzaher. 2025. Phy-Taylor: Partially Physics-Knowledge-Enhanced Deep Neural Networks via NN Editing. *IEEE Transactions on Neural Networks and Learning Systems* 36, 1 (Jan. 2025), 447–461. doi:10.1109/TNNLS.2023.3325432
- [38] Zhenjiang Mao, Siqi Dai, Yuang Geng, and Ivan Ruchkin. 2024. Zero-shot Safety Prediction for Autonomous Robots with Foundation World Models. *arXiv preprint arXiv:2404.00462* (2024).
- [39] Vincent Micheli, Eloi Alonso, and François Fleuret. 2022. Transformers are sample-efficient world models. *arXiv preprint arXiv:2209.00588* (2022).
- [40] Chen Min, Dawei Zhao, Liang Xiao, Yiming Nie, and Bin Dai. 2023. Uniworld: Autonomous driving pre-training via world models. *arXiv preprint arXiv:2308.07234* (2023).
- [41] Malte Mosbach, Jan Niklas Ewertz, Angel Villar-Corrales, and Sven Behnke. 2025. SOLD: Slot Object-Centric Latent Dynamics Models for Relational Manipulation Learning from Pixels. arXiv:2410.08822 [cs.LG] <https://arxiv.org/abs/2410.08822>
- [42] Kensuke Nakamura and Somil Bansal. 2023. Online update of safety assurances using confidence-based predictions. In *2023 IEEE International Conference on Robotics and Automation (ICRA)*. IEEE, 12765–12771.
- [43] Andi Peng, Mycal Tucker, Eoin Kenny, Noga Zaslavsky, Pulkit Agrawal, and Julie A Shah. 2024. Human-guided complexity-controlled abstractions. *Advances in Neural Information Processing Systems* 36 (2024).
- [44] Jordan Peper, Zhenjiang Mao, Yuang Geng, Siyuan Pan, and Ivan Ruchkin. 2025. Four Principles for Physically Interpretable World Models. *arXiv preprint arXiv:2503.02143* (2025).
- [45] Ali Razavi, Aaron Van den Oord, and Oriol Vinyals. 2019. Generating diverse high-fidelity images with vq-vae-2. *Advances in neural information processing systems* 32 (2019).
- [46] Ivan Ruchkin, Matthew Cleaveland, Radoslav Ivanov, Pengyuan Lu, Taylor Carpenter, Oleg Sokolsky, and Insup Lee. 2022. Confidence composition for monitors of verification assumptions. In *2022 ACM/IEEE 13th International Conference on Cyber-Physical Systems (ICCP)*. IEEE, 1–12.
- [47] Tim Salzmann, Boris Ivanovic, Punarjay Chakravarty, and Marco Pavone. 2020. Trajectron++: Dynamically-feasible trajectory forecasting with heterogeneous data. In *Computer Vision—ECCV 2020: 16th European Conference, Glasgow, UK, August 23–28, 2020, Proceedings, Part XVIII 16*. Springer, 683–700.
- [48] Dylan Sam, Rattana Pukdee, Daniel P Jeong, Yewon Byun, and J Zico Kolter. 2024. Bayesian neural networks with domain knowledge priors. *arXiv preprint arXiv:2402.13410* (2024).
- [49] Younggyo Seo, Danijar Hafner, Hao Liu, Fangchen Liu, Stephen James, Kimin Lee, and Pieter Abbeel. 2023. Masked world models for visual control. In *Conference on Robot Learning*. PMLR, 1332–1344.

- [50] Xingjian Shi, Zhourong Chen, Hao Wang, Dit-Yan Yeung, Wai-Kin Wong, and Wang-chun Woo. 2015. Convolutional LSTM network: A machine learning approach for precipitation nowcasting. *Advances in neural information processing systems* 28 (2015).
- [51] Kaustubh Sridhar, Souradeep Dutta, James Weimer, and Insup Lee. 2023. Guaranteed conformance of neurosymbolic models to natural constraints. In *Learning for Dynamics and Control Conference*. PMLR, 76–89.
- [52] Renukanandan Tumu, Lars Lindemann, Truong Nghiem, and Rahul Mangharam. 2023. Physics constrained motion prediction with uncertainty quantification. In *2023 IEEE Intelligent Vehicles Symposium (IV)*. IEEE, 1–8.
- [53] Aaron Van Den Oord, Oriol Vinyals, et al. 2017. Neural discrete representation learning. *Advances in neural information processing systems* 30 (2017).
- [54] Ari Viitala, Rinu Boney, Yi Zhao, Alexander Ilin, and Juho Kannala. 2021. Learning to drive (L2D) as a low-cost benchmark for real-world reinforcement learning. In *2021 20th International Conference on Advanced Robotics (ICAR)*. IEEE, 275–281.
- [55] Masaki Waga, Ezequiel Castellano, Sasinee Pruekprasert, Stefan Klikovits, Toru Takisaka, and Ichiro Hasuo. 2022. Dynamic shielding for reinforcement learning in black-box environments. In *International Symposium on Automated Technology for Verification and Analysis*. Springer, 25–41.
- [56] Chuan Wen, Xingyu Lin, John So, Kai Chen, Qi Dou, Yang Gao, and Pieter Abbeel. 2023. Any-point trajectory modeling for policy learning. *arXiv preprint arXiv:2401.00025* (2023).
- [57] Philipp Wu, Alejandro Escontrela, Danijar Hafner, Pieter Abbeel, and Ken Goldberg. 2023. Daydreamer: World models for physical robot learning. In *Conference on robot learning*. PMLR, 2226–2240.
- [58] Yifan Xue, Michael Ding, and Xinghua Lu. 2019. Supervised vector quantized variational autoencoder for learning interpretable global representations. *arXiv preprint arXiv:1909.11124* (2019).
- [59] Ziyang Yan, Wenzhen Dong, Yihua Shao, Yuhang Lu, Liu Haiyang, Jingwen Liu, Haozhe Wang, Zhe Wang, Yan Wang, Fabio Remondino, et al. 2024. Renderworld: World model with self-supervised 3d label. *arXiv preprint arXiv:2409.11356* (2024).
- [60] Mengyue Yang, Furui Liu, Zhitang Chen, Xinwei Shen, Jianye Hao, and Jun Wang. 2021. Causalvae: Disentangled representation learning via neural structural causal models. In *Proceedings of the IEEE/CVF conference on computer vision and pattern recognition*. 9593–9602.
- [61] Dingling Yao, Caroline Muller, and Francesco Locatello. 2024. Marrying causal representation learning with dynamical systems for science. *Advances in Neural Information Processing Systems* 37 (2024), 71705–71736.
- [62] Zhe Zhao, Mengshi Qi, and Huadong Ma. 2024. Decomposed Vector-Quantized Variational Autoencoder for Human Grasp Generation. In *European Conference on Computer Vision*. Springer, 447–463.
- [63] Wenzhao Zheng, Weiliang Chen, Yuanhui Huang, Borui Zhang, Yueqi Duan, and Jiwen Lu. 2024. Occworld: Learning a 3d occupancy world model for autonomous driving. In *European conference on computer vision*. Springer, 55–72.
- [64] Weiheng Zhong and Hadi Meidani. 2023. PI-VAE: Physics-Informed Variational Auto-Encoder for stochastic differential equations. *Computer Methods in Applied Mechanics and Engineering* 403 (2023), 115664. doi:10.1016/j.cma.2022.115664
- [65] Sicheng Zuo, Wenzhao Zheng, Yuanhui Huang, Jie Zhou, and Jiwen Lu. 2024. Gaussianworld: Gaussian world model for streaming 3d occupancy prediction. *arXiv preprint arXiv:2412.10373* (2024).

## Appendix

**Model Architecture and Training Details.** This appendix provides detailed implementation specifications for the Physically Interpretable World Model (PIWM) and its four instantiations: intrinsic-continuous, intrinsic-discrete, extrinsic-continuous, and extrinsic-discrete. All variants follow the unified formulation introduced in Section 3, operating on the same dataset, the same weak supervision mechanism, and the same training objective.

*A. Vision Encoders and Decoders.* All variants share the same convolutional vision encoder  $\mathcal{E}_v$  and decoder  $\mathcal{D}_v$ . The encoder contains two convolutional layers with ReLU activations and maps each observation  $y_t$  to an intermediate latent vector  $z_t \in \mathbb{R}^{64}$ . The decoder  $\mathcal{D}_v$  mirrors this structure and reconstructs an image  $\hat{y}_{t+2}$  from a latent representation. Continuous variants use a standard  $\beta$ -VAE objective on  $z_t$  with  $\beta = 1$ , while discrete variants apply a VQ-VAE quantization layer with a codebook of 512 learnable embeddings of dimension 64, trained using a commitment weight of  $\beta = 0.25$ .

*B. Physical Encoder  $\mathcal{E}_p$ .* In extrinsic architectures, the interpretable latent state is produced by a physical encoder  $\mathcal{E}_p$  applied to the intermediate visual latent:

$$z_t^* = \mathcal{E}_p(z_t).$$

This module is implemented as a Transformer encoder with two layers, four attention heads per layer, a model dimension of 128, and a feedforward width of 512. Mean pooling across tokens is followed by a linear projection to produce the final interpretable state  $z_t^*$ . The physical encoder is trained entirely via the interpretability loss  $\mathcal{L}_{\text{interp}}(z_t^*, \Xi_t)$ .

*C. Intrinsic Representation Learning.* Intrinsic variants produce the interpretable latent state directly from images,

$$z_t^* = \mathcal{E}(y_t),$$

without an intermediate latent or a separate physical encoder. For intrinsic-continuous models,  $\mathcal{E}$  outputs the parameters of a Gaussian distribution over the latent  $z_t^* \in \mathbb{R}^{64}$ , where a fixed subset of dimensions corresponds to the physical component  $z_{p,t}^*$ . The loss combines reconstruction, interpretability alignment, and KL regularization following the  $\beta$ -VAE formulation.

For intrinsic-discrete models, a VQ-VAE codebook of 512 embeddings is used. Each embedding vector is partitioned as  $\mathbf{e}_k = [\mathbf{e}_k^p, \mathbf{e}_k^c]$ , matching the structure in Section 3. The interpretable state is computed from the physical portion of the selected codebook entry, and the interpretability loss is applied directly to this physical component.

*D. Dynamics Model.* All variants share the same structured second-order latent dynamics model described in Section 3:

$$z_{t+2}^* = \phi_\theta(z_t^*, z_{t+1}^*, a_t).$$

The functional form of  $\phi_\theta$  is derived from the physics of each environment (e.g., kinematics), with only the parameters  $\theta$  being learnable. Depending on the environment,  $\phi_\theta$  contains between 4 and 10 unknown physical parameters. A two-step initialization window ( $z_t^*, z_{t+1}^*$ ) provides the required derivative information for prediction, such as implicit velocities.

At each time step, weak supervision consists of a set of  $L = 50$  proxy samples  $\Xi_t = \{\xi_t^{(l)}\}$  drawn from the unknown distribution  $p(x_t)$ . The dynamics loss is computed as

$$\mathcal{L}_{\text{dyn}} = \|z_{t+H}^* - \hat{\mu}_{\xi_{t+H}}\|_2^2,$$

where  $\hat{\mu}_{\xi_t}$  is the empirical sample mean of  $\Xi_t$ .

*E. Loss Functions.* All variants are trained using the unified objective:

$$\mathcal{L} = \mathcal{L}_{\text{rec}} + \lambda_1 \mathcal{L}_{\text{interp}} + \lambda_2 \mathcal{L}_{\text{dyn}} + \lambda_3 \mathcal{L}_{\text{reg}}.$$

The reconstruction loss is mean squared error in image space:

$$\mathcal{L}_{\text{rec}} = \|\mathcal{D}_v(z_{t+2}) - y_{t+2}\|_2^2.$$

The interpretability loss uses the weak supervision samples:

$$\mathcal{L}_{\text{interp}} = \|z_{p,t}^* - \hat{\mu}_{\xi_t}\|_2^2.$$

Continuous variants use KL regularization consistent with the  $\beta$ -VAE formulation, whereas discrete variants use VQ-VAE codebook and commitment losses, matching the structure defined in Section 3.

*F. Training Setup.* All models are trained using the Adam optimizer with batch size 32. Continuous variants use an initial learning rate of  $10^{-4}$ , and discrete variants use  $10^{-3}$  due to the stochasticity introduced by quantization. A cosine decay schedule with 5 warmup epochs is applied. Training proceeds for up to 200 epochs, with early stopping after 20 epochs of no validation improvement. Gradient norms are clipped at 1.0 for stability. Evaluation uses 30-step prediction rollouts in latent space, decoding to images only when needed.

Weak supervision is applied consistently across noise settings  $\delta \in \{0\%, 5\%, 10\%\}$ .

*G. Summary of Differences Between Variants.* Intrinsic models produce  $z_t^*$  directly from observations, whereas extrinsic models obtain  $z_t^*$  through the composition  $z_t^* = \mathcal{E}_p(\mathcal{E}_v(y_t))$ . Continuous variants use Gaussian latent parameterizations, and discrete variants use a VQ-VAE codebook with 512 entries. Across all variants, the interpretable component of the latent occupies a fixed subset of dimensions. All models share identical dynamics functions  $\phi_\theta$  and training losses.

*H. Architectural Details in Text.* All models use a shared two-layer CNN vision encoder and decoder producing a 64-dimensional latent space. Continuous variants use Gaussian latents with a KL penalty, while discrete variants use a 512-entry VQ-VAE codebook trained with a commitment weight of  $\beta = 0.25$ . Extrinsic variants include a two-layer Transformer physical encoder with model dimension 128. Intrinsic variants instead embed the physical portion directly into  $z_t^*$ . The dynamics model learns between 4 and 10 environment-specific parameters using 50 weak supervision samples per time step.

*I. Training Hyperparameters in Text.* All experiments use batch size 32, cosine learning-rate decay with 5 warmup epochs, a maximum of 200 epochs with patience 20, and gradient clipping at 1.0. Rollouts span 30 steps in latent space. All environments use the same 60,000-trajectory dataset and weak supervision noise levels  $\delta \in \{0\%, 5\%, 10\%\}$ .

**Architecture for the Extrinsic-Discrete Variant.** This section provides an expanded diagram of the *extrinsic-discrete* variant

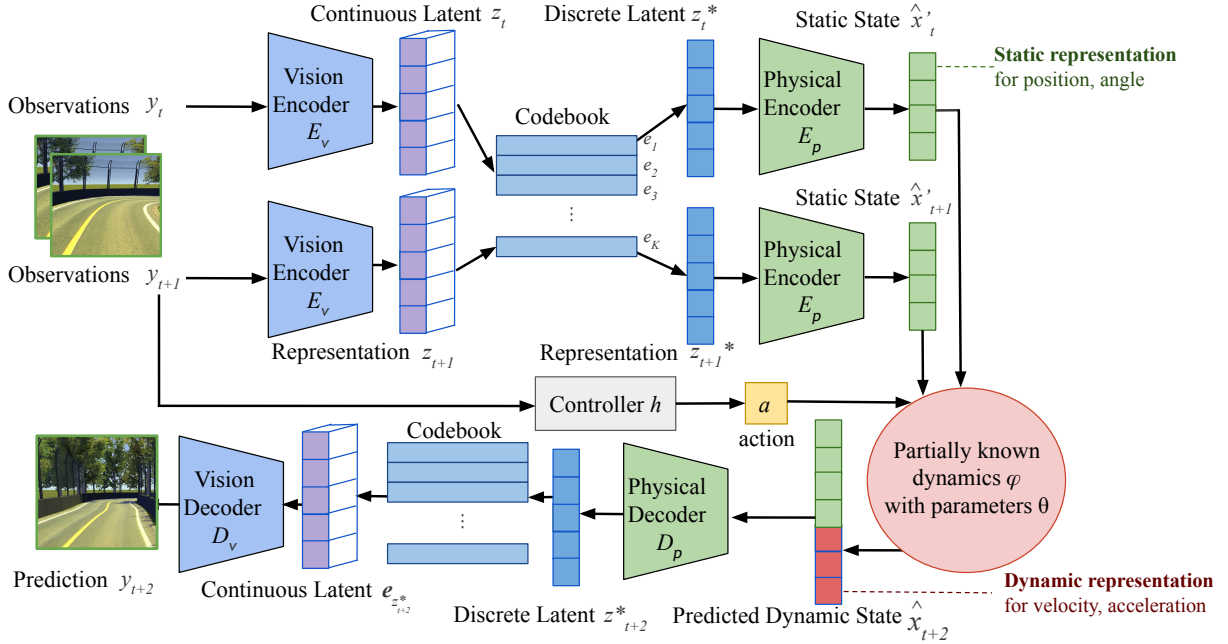


**Figure 7: Extrinsic-discrete PIWM architecture.** The vision encoder  $E_v$  produces latents  $z_t$ , which are quantized to  $z_t^*$  and mapped to physical states by  $E_p$ . The dynamics model  $\phi_\theta$  predicts  $\hat{x}_{t+2}$  from two physical states and action  $a_t$ , and the decoders  $D_p$  and  $D_v$  reconstruct the predicted observation.

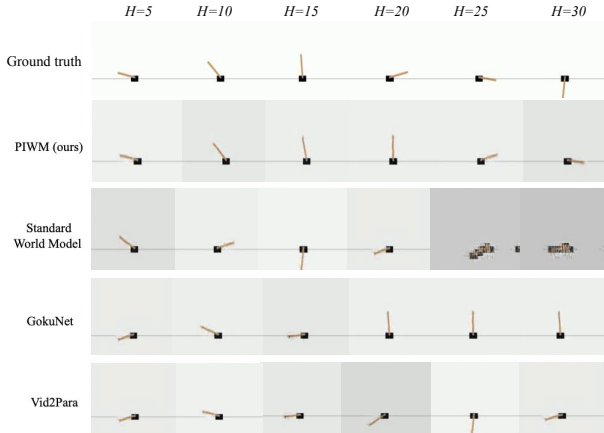


**Figure 8: Qualitative comparison of 30-step trajectory roll-outs under  $\delta = 5\%$  of Cart Pole.**

of PIWM, which is used in our experiments. Unlike intrinsic variants, the extrinsic pipeline decouples visual perception from physical interpretation: a VQ-based vision autoencoder first produces a discrete latent representation, after which a dedicated physical encoder extracts the interpretable physical state. This figure visualizes the complete data flow from raw observations to discrete latents, physical state estimation, structured dynamics prediction, and final reconstruction.

**Controller Performance on Reconstructions.** To assess whether PIWM variants preserve task-relevant visual information, we evaluate how well reconstructed observations  $\hat{y}_t$  support action prediction when passed through the environment’s original controller  $h$ . Table 2 summarizes controller performance (action RMSE for Donkey Car; action accuracy for Lunar Lander and CartPole) for all four architectural variants and all supervision noise levels. These results provide a complementary diagnostic showing how the different latent designs affect the quality of reconstructed observations for downstream control.

**Table 2: Controller Performance on Reconstructed Observations Across All Variants and Noise Levels**

Case	Input Type	Latent Space	Supervision Noise Level ( $\delta$ )		
			0%	5%	10%
Donkey Car (Action RMSE ↓)	One-Stage (Intrinsic)	Continuous	0.12 ± 0.04	0.13 ± 0.04	0.15 ± 0.05
		Discrete	0.21 ± 0.15	0.29 ± 0.16	0.32 ± 0.20
	Two-Stage (Extrinsic)	Continuous	0.15 ± 0.05	0.16 ± 0.05	0.22 ± 0.06
		Discrete	0.15 ± 0.04	0.17 ± 0.05	0.19 ± 0.05
Lunar Lander (Action Acc. ↑)	One-Stage (Intrinsic)	Continuous	93.0% ± 1.8%	90.5% ± 2.0%	87.1% ± 2.2%
		Discrete	85.5% ± 2.5%	82.1% ± 2.8%	78.3% ± 3.1%
	Two-Stage (Extrinsic)	Continuous	86.2% ± 2.4%	83.5% ± 2.6%	80.0% ± 2.9%
		Discrete	91.5% ± 2.1%	88.6% ± 2.3%	84.5% ± 2.5%
Cart Pole (Action Acc. ↑)	One-Stage (Intrinsic)	Continuous	98.0% ± 1.0%	96.5% ± 1.2%	94.0% ± 1.5%
		Discrete	95.0% ± 1.6%	91.5% ± 2.0%	87.2% ± 2.5%
	Two-Stage (Extrinsic)	Continuous	95.5% ± 1.5%	92.0% ± 1.8%	88.0% ± 2.2%
		Discrete	97.2% ± 1.1%	95.0% ± 1.4%	92.5% ± 1.8%